JOURNAL OF GUIDANCE, CONTROL, AND DYNAMICS
Vol. 18, No. 4, July–August 1995

Satellite Autonomous Navigation Based on Magnetic Field Measurements

Gil Shorshi* and Itzhack Y. Bar-Itzhack†
Technion—Israel Institute of Technology, Haifa, 32000 Israel

This paper presents a near-Earth (less than 1000 km altitude) satellite autonomous navigation and orbit determination method using measurements of the Earth magnetic field. An orbit state vector comprised of six Keplerian elements enables the estimation of the instantaneous orbital elements by a relatively simple extended Kalman filter algorithm. The satellite position and velocity are computed as a function of the estimated orbital elements. Several algorithms were developed. The basic algorithm uses a "measurement" of the magnetic field magnitude. Consequently, this algorithm is independent of attitude information. Simulation tests yielded accurate Keplerian element estimation and a few kilometers of position estimation error. More complicated algorithms that estimate drag and/or utilize attitude information were tested. The basic algorithm was successfully applied to real Earth Radiation Budget Satellite data, and a modified version of this algorithm was applied to Gamma Ray Observatory magnetometer readings to yield estimates of the orbital elements and the position and velocity. In both cases of real satellite navigation, the position was estimated within a few tens of kilometers.

I. Introduction

SATELLITE orbit determination and navigation problems have been investigated for the last three decades. As a result of the improvement obtained in computation and estimation methods of orbit dynamic models and, mainly, in the improvement of measuring systems, it is possible, today, to identify satellite position with high accuracy. Position determination error of a few meters or better can be reached, but reliance on ground tracking stations or the Global Positioning System (GPS) is necessary.

The rapid development of onboard computers in the last 15 years (which has resulted in increased computation power and flexibility together with reduced hardware dimension and weight) has contributed to an increased interest in autonomous satellite operation. Considering the expected growth of space "traffic" in the future, satellite autonomy is an important factor in decreasing operation costs. From the military standpoint, it facilitates operation in a hostile EM environment, when jamming or danger of discovery exist. Since the 1960s, a variety of autonomous navigation systems, ranging from navigation by Earth landmarks to celestial navigation, have been proposed and explored.[1] The predicted accuracy of these systems, ranging from 100 m to a few kilometers, can be adequate for civilian satellites. Military accuracy requirements, however, such as those of the Strategic Defense Initiative (SDI), are more severe. These accuracies can be achieved using the Global Positioning System (GPS), but this method of navigation is semiautonomous because it depends on communication with other satellites.

In the last three years, a new method for autonomous navigation using magnetometer data has been investigated. This method is based on the fact that Earth's magnetic field is a fairly well-modeled field whose intensity and direction are functions of position. The yearly variations can be accounted for to a reasonable degree of accuracy. Since position and velocity are functions of low-Earth-orbit (LEO) elements, it is possible to estimate those elements that are observable by applying an extended Kalman filter (EKF) to effective measurements, defined as the difference between the measured and estimated magnetic field data. The estimated magnetic field is computed as a function of the estimated position. This is possible since this field is a function of position. This function is known quite well. It is called the International Geomagnetic Reference Field (IGRF) model. Results obtained with simulated[2,3] and real[4] data have been reported. The algorithm of Ref. 4, for example, employed the square root information filter (SRIF) implementation of the EKF using a nine-element state vector. The state vector included the velocity magnitude and direction, the position in spherical coordinates, and aerodynamic coefficients. Position accuracy of a few kilometers has been achieved with simulated data and with data from the Magnetic Field Satellite (MAGSAT). However, as pointed out by the authors, the high accuracy achieved with MAGSAT data was atypical.[4] In order to overcome the considerable measurement disturbance in satellites other than MAGSAT, a batch least-squares filter was developed in Ref. 4 that estimates orbital Keplerian-type elements and the magnetometer biases. As reported in Ref. 4, tests of the batch algorithm with data obtained from the Dynamics Explorer-2 spacecraft resulted in position accuracies of 18 km and better. Peak errors of 125 km were obtained from the application of the batch algorithm to data from the Low-Power Atmosphere Compensation Experiment spacecraft.

In this paper we present algorithms for orbit determination and satellite navigation that yield, in simulations, position estimation accuracy similar to that achieved by simulations in Refs. 2 and 3, with less complexity. Modifications have been made to handle, recursively, significant biases and low-frequency measurement disturbances encountered when using real satellite data. Position estimation accuracy of a few tens of kilometers was achieved when using data measured by magnetometers mounted on ERBS and GRO satellites.

II. Orbit and Measurement Simulation

The design of an EKF for orbit determination and navigation started with simulated data. Accordingly, the satellite orbit and noisy magnetometer measurements were simulated. The orbit simulation equations were based on Euler's variation-of-parameters method.[5] This method yields the reference trajectory expressed by its instantaneous Keplerian elements. The equations included only J_2 oblateness and drag terms. The latter have the dominant effect on near-Earth orbits. It was reasonable not to include other elements such as J_3, sun, and moon effects because the dynamic model of the filter in our basic navigation algorithm did not include the drag influence; thus, it is illogical to account for the secondary effects, mentioned above, which are negligible in comparison with the drag effect, which was not included in the filter model.

The simulated magnetometer measurements were computed using the eighth-order 1985 IGRF model.[6] This computation generated the components of the magnetic field vector resolved in the body

Received Aug. 23, 1993; revision received June 24, 1994; accepted for publication Sept. 14, 1994.

*Graduate Student, Faculty of Aerospace Engineering.
†Sophie and William Shamban Professor of Aerospace Engineering, Faculty of Aerospace Engineering.

coordinate system. In our simulation, the body axes coincided with the orbit axes. A zero-mean Gaussian white noise was added to each component. The simulated measurement noise reflected the dominant disturbance caused by the inaccuracy of the magnetic field model (sensor bias has not been included in the first stage of the research).

III. Navigation Algorithm Description

Several algorithms were developed, a basic one and more complicated ones. The latter algorithms were developed in order to examine the accuracy improvement achieved when unmodeled effects were estimated and when attitude information was used. The algorithms are described next.

A. Basic Algorithm

As mentioned before, the orbit dynamic model in the basic filter algorithm did not include the simulated drag effect. The effect of J_2 was used in the propagation of the state estimate but not in the covariance propagation. As will be shown, this practice was justified. In this algorithm "measurement" of the magnetic field vector magnitude was used. The advantages of this algorithm are in its simplicity and in the independence of attitude information. Due to the nonlinearity of the dynamic and measurement equations, an EKF was used to estimate the satellite orbital elements. The satellite position and velocity were computed as functions of the estimated orbital elements.

1. State Vector

The filter state vector consisted of the classical six Keplerian elements:

$$X^T = [a,\ e,\ i,\ \Omega,\ \omega,\ \theta] \tag{1}$$

where a is the semimajor axis, e is the eccentricity, i is the inclination, Ω is the right ascension of the ascending node, ω is the argument of perigee, and θ is the true anomaly.

This state vector selection has three advantages:

1) The state variables (excluding θ) change very little along the orbit.

2) Since the main part of the dynamics of θ results from the central gravity force, the dynamics can be adequately described by a relatively simple differential equation. This property simplifies the propagation of the filter covariance matrix.

3) The state vector estimation is an orbit determination process that produces directly the instantaneous orbital element estimates.

As a result of these qualities, the EKF implementation is relatively simple, reducing the computation complexity and the execution time.

2. Update Stage

The measurement model is described by the equation

$$y_k = N(\tilde{\boldsymbol{B}}(\boldsymbol{X}_k, t_k)) + v_k \tag{2}$$

where $N(\cdot)$ is the norm operator, $\tilde{\boldsymbol{B}}$ is the magnetic field vector according to the 1985 IGRF model, and v_k is a zero-mean Gaussian white noise whose variance is r_k.

The update equations are[7]

$$\hat{\boldsymbol{X}}_k(+) = \hat{\boldsymbol{X}}_k(-) + K_k[y_k - N(\tilde{\boldsymbol{B}}(\hat{\boldsymbol{X}}_k(-), t_k))] \tag{3}$$

where the gain matrix K_k (6×1) is

$$K_k = P_k(-)H_k^T\left[H_k P_k(-) H_k^T + r_k\right]^{-1} \tag{4}$$

The measurement matrix H_k (row matrix in this case) is computed using the chain rule:

$$H_k = \left.\frac{\partial N(\tilde{\boldsymbol{B}})}{\partial \boldsymbol{X}}\right|_{\hat{\boldsymbol{X}}_k(-),t_k} = \left.\frac{\partial N(\tilde{\boldsymbol{B}})}{\partial \tilde{\boldsymbol{B}}}\frac{\partial \tilde{\boldsymbol{B}}}{\partial \boldsymbol{R}}\frac{\partial \boldsymbol{R}}{\partial \boldsymbol{X}}\right|_{\hat{\boldsymbol{X}}_k(-),t_k} \tag{5}$$

where $\boldsymbol{R}$ is the position vector in spherical coordinates. The partial derivatives $\partial \boldsymbol{R}/\partial \boldsymbol{X}$ are computed analytically according to the spherical geometry relations and $\partial \tilde{\boldsymbol{B}}/\partial \boldsymbol{R}$ according to the magnetic field model equations (see Ref. 8 for details). The estimation error covariance matrix is updated as follows:

$$P_k(+) = [I - K_k H_k]P_k(-)[I - K_k H_k]^T + K_k r_k K_k^T \tag{6}$$

3. Propagation Stage

The updated estimate of the state vector, $\hat{\boldsymbol{X}}_k(+)$, is propagated from time t_k to t_{k+1} by numerical integration of the continuous nonlinear dynamic equation:

$$\dot{\hat{\boldsymbol{X}}} = \boldsymbol{f}(\hat{\boldsymbol{X}}) \tag{7}$$

which includes the J_2 effect (as in the simulated orbit) but without drag influence on the orbit dynamics. (As will be shown, the inclusion of drag unnecessarily complicates the filter when the estimation of drag is not required).

The updated estimation error covariance matrix is propagated from time t_k to t_{k+1} using

$$P_{k+1}(-) = A_k(\hat{\boldsymbol{X}}_k(+))P_k(+)A_k^T(\hat{\boldsymbol{X}}_k(+)) + Q_k \tag{8}$$

where Q_k is the process noise covariance matrix (used for tuning purposes) and A_k the transition matrix approximation, which is computed using a first-order Taylor series expansion:

$$A_k(\hat{\boldsymbol{X}}_k(+)) = I + F_k(X)|_{\hat{\boldsymbol{X}}_k(+)}\Delta T \tag{9}$$

where ΔT is the time interval between measurements.

The Jacobian $F_k(\boldsymbol{X})$ is based on the following state equation, describing an orbit generated by a central force only:

$$\dot{\boldsymbol{X}} = \boldsymbol{g}(\boldsymbol{X}) = \begin{bmatrix} \boldsymbol{O}_{5\times 1} \\ \hline g_6(\boldsymbol{X}) \end{bmatrix} \tag{10a}$$

$$g_6(\boldsymbol{X}) = \frac{\sqrt{\mu_E}(1 + e\cos\theta)^2}{[a(1-e^2)]^{1.5}} \tag{10b}$$

where

$$\mu_E = 398{,}600\ \mathrm{km}^3/\mathrm{s}^2 \tag{10c}$$

is the Earth gravitational parameter. Using this model, the Jacobian calculations were simplified considerably:

$$F_k(\boldsymbol{X}) = \frac{\partial g(\boldsymbol{X})}{\partial \boldsymbol{X}} = \begin{bmatrix} \multicolumn{6}{c}{O_{5\times 6}} \\ \hline F_{(6,1)} & F_{(6,2)} & 0 & 0 & 0 & F_{(6,6)} \end{bmatrix} \tag{11a}$$

where

$$F_{(6,1)} = \frac{\partial g_6}{\partial a} = -\frac{1.5}{a}g_6(\boldsymbol{X}) \tag{11b}$$

$$F_{(6,2)} = \frac{\partial g_6}{\partial e} = \left[\frac{3e}{1-e^2} + \frac{2\cos\theta}{1+e\cos\theta}\right]g_6(\boldsymbol{X}) \tag{11c}$$

$$F_{(6,6)} = \frac{\partial g_6}{\partial \theta} = -\frac{2e\sin\theta}{1+e\cos\theta}g_6(\boldsymbol{X}) \tag{11d}$$

4. Filter Divergence

Tests of the basic algorithm with simulated data of a typical near-Earth orbit resulted in a divergence of the position estimation error after 25 revolutions (Fig. 1). The EKF divergence is typical of orbit determination applications.[9] This is due to the long time of operation. In our case the divergence was caused by the error in the filter dynamic model, which resulted from the omission of the drag effect that was included in the simulation. During the filter operation, elements in the covariance matrix became smaller than they should have been. Consequently, the filter gain was typically not large enough to assign adequate weight to the innovations. In order to keep the basic algorithm simple, a lower bound was imposed on a few elements of the main diagonal in the filter covariance matrix. Consequently, the filter gain remained large enough and the filter divergence was eliminated.

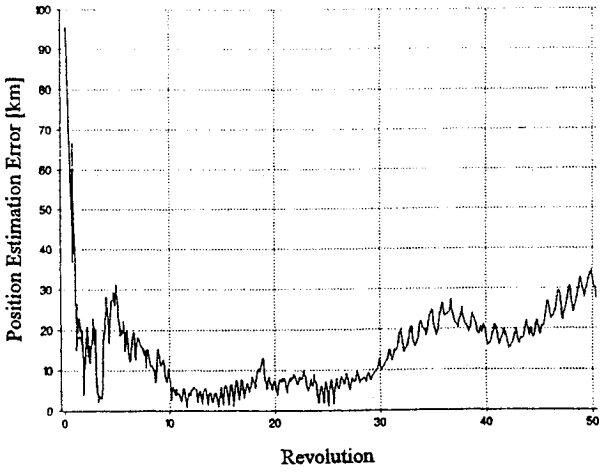

Fig. 1 Divergence of position estimation error (basic algorithm operating on simulated data).

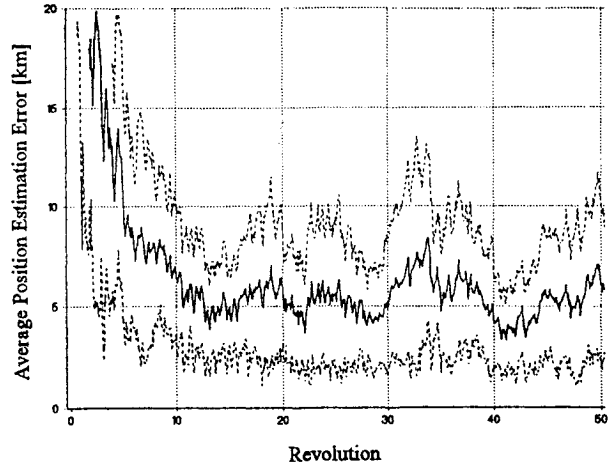

Fig. 2 Average position estimation error (basic algorithm operating on simulated data).

B. Algorithm with Drag Estimation

In this algorithm a satellite constant drag coefficient was added to the state vector defined in Eq. (1), and its estimated value was used in the propagation of the estimated state vector. This algorithm was developed in order to examine drag coefficient estimation using the magnetic field measurements and because it gave the best navigation performance. The latter is a result of the achieved identity between the design and truth models.[7] The calculation of the transition matrix in this case was more complicated (see Ref. 8). It was based on the state equation of a central force orbit with only drag effects. As before, the J_2 effect was used in the propagation of the state estimate, but not in the covariance propagation.

C. Algorithm Using Attitude Information

Satellite attitude is typically estimated on board during its mission. Attitude information enables state updates using measurement of the magnetic field vector components. The measurement model is the sum of zero-mean, Gaussian, white-noise elements and the components of the magnetic field vector resolved in body axes. The use of three component measurements complicated the measurement matrix computation (see Ref. 8). As in the basic algorithm, here too a divergence prevention measure was needed.

IV. Results Obtained with Simulated Orbits

The navigation algorithms were tested with simulated data of a typical near-Earth orbit. The sensitivity of the basic algorithm performance in different operational conditions was examined.

A. Results Obtained on Typical Orbit

Simulated data were generated for a typical orbit having a semimajor axis of 7000 km, eccentricity of 0.05, and 50 deg inclination angle. The satellite drag ballistic coefficient was assumed to be 50 kg/m^2. Measurement noise with 2 mG (200 nT) standard deviation was added to each component of the magnetic field vector. The sampling time interval was 30 s (194 samplings per revolution).

1. *Results of Basic Algorithm*

The position estimation error obtained when the basic algorithm was applied to the typical orbit data is plotted in Fig. 2. The solid line is the position estimation error averaged over 25 realizations (using different noise generator seeds). The dotted lines are plotted at plus and minus the standard deviation of the error signal.

A typical convergence pattern of the estimation error can be observed. In this case of the basic algorithm, the position estimation error was reduced from an initial value of more than 1000 km to a level of around 5 km in its steady state. The average estimation error of the x axis (inertial geocentric) velocity component is plotted in Fig. 3. Accurate identification of the orbital elements led to this navigation performance. As an example, the semimajor axis average estimation error is presented in Fig. 4.

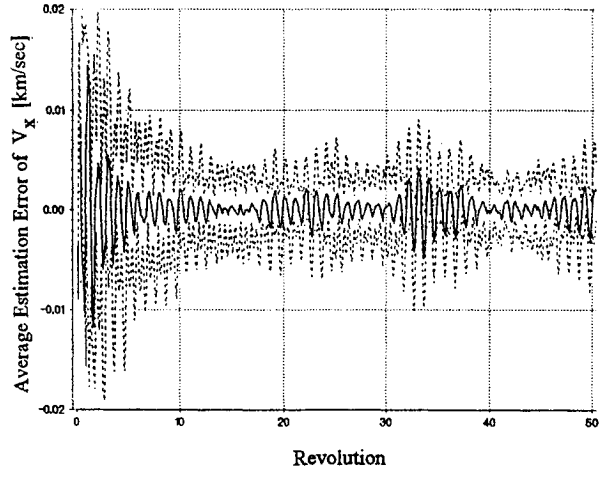

Fig. 3 Average estimation error of V_x (basic algorithm operating on simulated data).

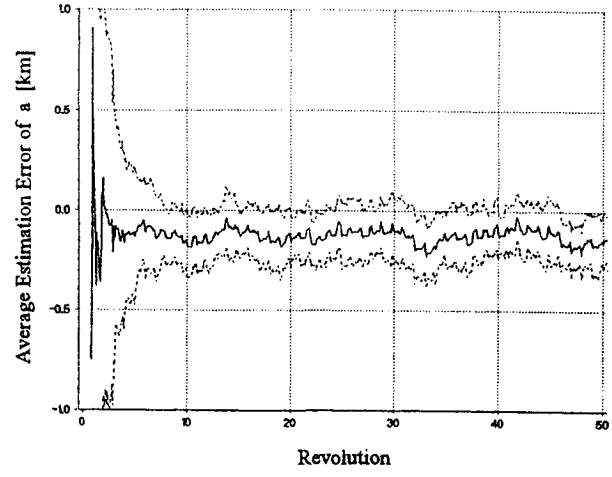

Fig. 4 Average estimation error of a (basic algorithm operating on simulated data).

An estimation accuracy of a few hundredths of degrees was observed in the case of the angular orbital elements. The eccentricity was estimated, yielding an estimation error standard deviation of 0.08% of the real eccentricity.

2. *Results of Nonbasic Algorithm*

The simulated orbit data, which were generated for the typical orbit (defined at the beginning of this section), were used to examine

the influence of drag estimation and use of attitude information on the resulting estimation accuracies. It was found that the drag coefficient can be well estimated. The use of this estimated drag coefficient in the estimated state vector update improved orbit determination and navigation accuracies only a little. However, when attitude information was used, considerable reductions of the estimation error convergence time and level were observed. The average steady-state position estimation error was around 1.8 km with small dispersions. The standard deviation of the average velocity estimation error was less than 0.002 km/s. These remarkable results are due mainly to the improved accuracy in the estimation of the angular elements.

B. Performance Sensitivity of Basic Algorithm

The influence of the operation conditions on the navigation accuracies was examined using the basic algorithm. It was found that the filter had a low tuning sensitivity. In higher altitudes (e.g., larger semimajor axis), the navigation was more accurate, in spite of the relative weakness of Earth's magnetic field. This was attributed to the little effect the drag has on the orbit. We observed that the navigation performance improved with increased inclination angle. This is so because, in highly inclined orbits, a satellite passes through more nonsymmetric regions of Earth's magnetic field. This fact enhances orbit identification using magnetic field measurements.

In cases of very low eccentricity (near-circular) orbits, the navigation accuracies degrade. The reason for this is that in such cases ω and θ are unobservable elements. However their sum, which is what we really need for navigation, is observable.

V. Application to Real Satellite Data

Data obtained from the satellites ERBS and GRO were used to test the algorithms with real data. In addition to other information, the data included magnetometer measurements, attitude information, and satellite position from ground tracking stations. The estimated orbital elements, as well as position and velocity, were compared with their best known values in order to obtain an evaluation of the corresponding estimation errors. It should be noted that, although these tests were performed off-line on the ground with past data, these tests do not differ from on-line on-board flight tests and therefore should be viewed as such.

A. ERBS Real Data

ERBS (Earth Radiation Budget Satellite) was launched in October 1984 in order to collect scientific data. The data used in our test were recorded in November 1986 over two revolutions when the ERBS orbit had the following approximate characteristics: semimajor axis of 6975 km, eccentricity of 0.002, and inclination of 56.7 deg. The data included time, position, the transformation matrix from inertial geocentric axes to body axes, and three bias-cleaned magnetometer measurements. The disturbance ϵ in the "measurement" of the magnitude of the magnetic field was computed as follows:

$$\epsilon = N(\boldsymbol{B}_{\mathrm{ms}}) - N(\tilde{\boldsymbol{B}}(\boldsymbol{R}_{\mathrm{ms}}, t_{\mathrm{ms}})) \tag{12}$$

where $\boldsymbol{B}_{\mathrm{ms}}$ is the measured magnetic field vector and $\boldsymbol{R}_{\mathrm{ms}}$ and t_{ms} are the ground-station tracked position vector and measured time, respectively.

Frequency-domain analysis of the resulting disturbance signal revealed that the disturbance had a white-noise nature suitable for processing by an EKF. However, similar calculations carried out for the measured magnetic field components (using the attitude information) resulted in a nonuniform disturbance signal characteristic. In addition, malfunctions were observed in one ERBS magnetometer, eliminating the ability of using the algorithms that utilize the magnetic field components.

Due to the fact that it is impossible to estimate the drag coefficient over two orbits only, we did not use the algorithm that estimates drag. Consequently, of the algorithms developed, we could test only the basic algorithm on ERBS data.

B. Results Obtained with Real ERBS Data

The position estimation error obtained when the basic algorithm was applied to ERBS data, with 32-s sampling intervals (about 181 samplings per revolution), is plotted in Fig. 5. The total position error was reduced from a level of 1000 km to 30–40 km in less than two revolutions. The orbital elements were estimated after less than one revolution and started to undergo their typical time behavior. More on ERBS results can be found in Bar-Itzhack and Shorshi.[10] The white-noise characteristics of the measurement disturbance enabled the successful use of the basic algorithm. Note that there was no need to limit the covariance decrease in order to check the divergence occurring due to the exclusion of the drag coefficient from the filter model. This was so because divergence is expected to occur only after some 25 revolutions and we had data of only 2 revolutions.

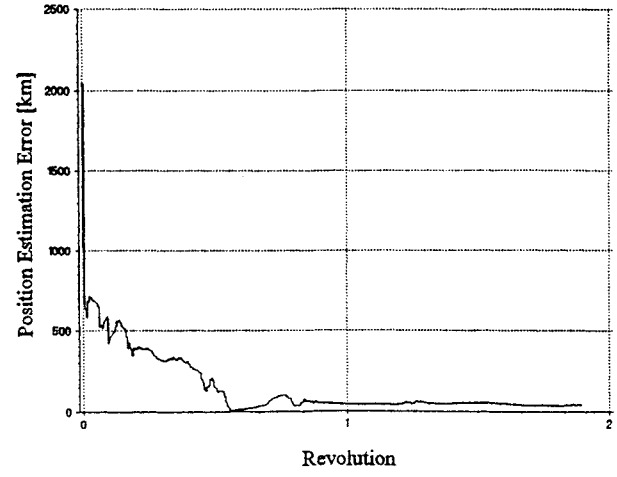

Fig. 5 Position estimation error (basic algorithm operating on ERBS data).

C. Results Obtained with Real GRO Data

The GRO satellite was launched in April 1991. Data recorded during almost seven revolutions of GRO on April 11, 1991, were used in our testing. The data included time, position, attitude quaternion from inertial geocentric to body axes, and three magnetometer readings. Some preprocessing of the data was carried out in order to prepare the data for use by the estimation algorithms. First, the effect of torquer moments on the magnetometer readings was removed as follows:

$$\boldsymbol{B}_{\mathrm{ms}} = \boldsymbol{B}_{rd} - C\boldsymbol{M} \tag{13}$$

where $\boldsymbol{B}_{rd}$ is the vector of magnetometer readings, $\boldsymbol{B}_{\mathrm{ms}}$ is the vector of "magnetometer measurements," C is a matrix of influence coefficients, and $\boldsymbol{M}$ is the vector of torquer moments. Second, in order to generate a reference for comparison purposes of the estimated orbital elements, an evaluation of the true elements was carried out as follows. An evaluation of GRO orbital elements was given by NASA-Goddard for the initial data point. It included the following values: a semimajor axis of 6836.266 km, an eccentricity of 0.0020669, and an inclination of 28.4957 deg. These values were used as initial values in an orbit simulation. This simulation generated orbital element time histories that were compared with the estimated values in order to evaluate the algorithm orbit determination quality.

As in the case of ERBS data, the magnetic field measurement disturbances [see Eq. (12)] were computed. The magnitude measurement disturbance as a function of the satellite revolutions is plotted in Fig. 6, in which considerable bias and low-frequency disturbance can be observed. This could be attributed to magnetometer error, magnetic field model inaccuracies, and position errors. The measurement disturbance of each magnetometer was examined too, yielding similar low-frequency characteristics with the addition of high-intensity (several milligauss) spikes. In the z-body axis direction, a bias of 4 mG was observed. It was the dominant contributor to the magnitude measurement disturbance bias. In order to obtain reasonable navigation performance, in spite of these considerable measurement disturbances, the algorithms were modified as described next.

D. Augmented Navigation Algorithm

The application of the basic navigation algorithm to GRO data yielded unacceptable position errors that ranged up to 200 km. They were caused by the considerable measurement disturbance. In order to improve the estimates, the disturbance signal was analyzed in the frequency domain. The resulting power spectral density (PSD) (Fig. 7) curve can be approximated by a descending line starting from a peak at zero frequency and leveling off at some frequency. This revealed the presence of a Markov process and a bias in the disturbance. The frequency at which the descending line levels off determines the time constant of the Markov process. An adequate model for the disturbance is shown in Fig. 8, where η is a bias component, w is a zero-mean white noise, and T is the correlation time. The output m represents the disturbance. The model is described analytically as follows:

$$\frac{\mathrm{d}}{\mathrm{d}t}\begin{bmatrix} m \\ \eta \end{bmatrix} = T^{-1}\begin{bmatrix} -1 & 1 \\ 0 & 0 \end{bmatrix}\begin{bmatrix} m \\ \eta \end{bmatrix} + T^{-1}\begin{bmatrix} w \\ 0 \end{bmatrix} \tag{14}$$

This model was added to the system dynamic model; consequently the augmented state vector $\boldsymbol{X}_a$ was

$$\boldsymbol{X}_a^T = [\boldsymbol{X}^T, m, \eta] \tag{15}$$

where $\boldsymbol{X}$ is the state vector defined in Eq. (1). As usual, if m and η are observable, the resulting algorithm, which we call an augmented basic algorithm, estimates m and η in addition to the orbital elements. The modified measurement model is described by the equation

$$y_k = N(\tilde{\boldsymbol{B}}(\boldsymbol{X}_k, t_k)) + m_k + v_k \tag{16}$$

The basic algorithm update equations were modified to include calibration of the magnetic field magnitude measurement:

$$\hat{\boldsymbol{X}}_{a_k}(+) = \hat{\boldsymbol{X}}_{a_k}(-) + K_{a_k}\{y_k - [N(\tilde{\boldsymbol{B}}(\hat{\boldsymbol{X}}_k(-), t_k)) + \hat{m}_k(-)]\} \tag{17}$$

where $K_{a_k}(8 \times 1)$ is computed with the measurement matrix H_{a_k} (row matrix in this case):

$$H_{a_k} = [H_k \mid 1 \quad 0] \tag{18}$$

The propagation of the orbital elements updated estimation, $\hat{\boldsymbol{X}}_k(+)$, is the same as in the basic algorithm. The propagation of the estimated states $\hat{m}$ and $\hat{\eta}$ is as follows:

$$\hat{m}_{k+1}(-) = \left(1 - \frac{\Delta T}{T_p}\right)\hat{m}_k(+) + \frac{\Delta T}{T_p}\hat{\eta}_k(+) \tag{19a}$$

$$\hat{\eta}_{k+1}(-) = \hat{\eta}_k(+) \tag{19b}$$

where ΔT is the time interval between measurements and T_p the correlation time (tuning parameter) of the disturbance Markov component.

The updated estimation error covariance matrix propagation includes use of a modified transition matrix approximations:

$$A_{a_k}(\hat{\boldsymbol{X}}_k(+)) = \left[\begin{array}{c:cc} A_k(\hat{\boldsymbol{X}}_k(+)) & O_{6\times 2} & \\ \hdashline & 1 - \Delta T/T_p & \Delta T/T_p \\ O_{2\times 6} & 0 & 1 \end{array}\right] \tag{20}$$

Naturally, the algorithm with attitude information that used magnetic field components as measurements was modified too. This required the addition of three pairs of new state variables to the state vector $\boldsymbol{X}$. Each pair consisted of m and η for the corresponding component of the magnetic field measurement.

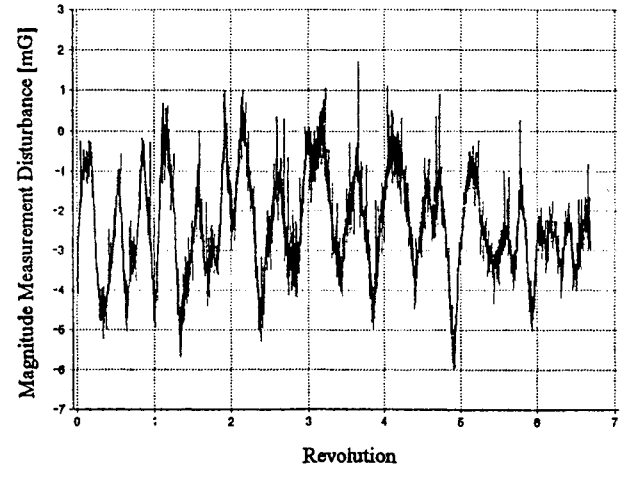

Fig. 6 GRO magnetic field magnitude "measurement" disturbance.

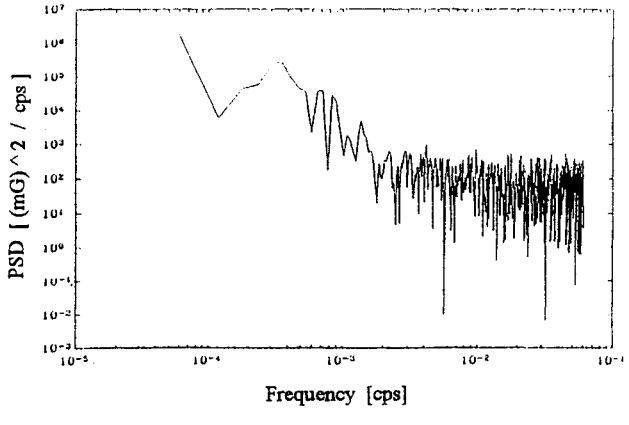

Fig. 7 Power spectral density of GRO magnetic field magnitude "measurement" disturbance.

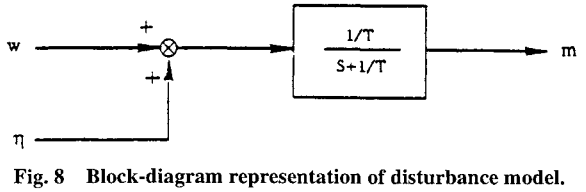

Fig. 8 Block-diagram representation of disturbance model.

E. Results Obtained with GRO Data

The application of the augmented navigation algorithms to GRO real data, yielded acceptable results. The capability of the algorithms to estimate, recursively, high-intensity measurement disturbance was proven. (Note that in Ref. 4 only batch filters could handle the disturbance.) This is shown in the following results.

1. Results of Augmented Basic Algorithm

The position estimation error obtained with an 8.2-s sampling interval (about 687 samplings per revolution) is presented in Fig. 9. A reduction from an initial value of 1500 km to a level of 100 km after one revolution of data processing can be seen. In the next revolutions the error signal was oscillatory, with relatively high amplitude. Toward the sixth revolution the signal characteristics were changed, and it reached a level of 20–40 km. Accurate velocity estimation was obtained. The estimation error of the x axis (inertial-geocentric) velocity component is plotted in Fig. 10.

The estimated GRO orbital elements are plotted (solid line) in Figs. 11a–11e. The reference (dotted line) represents the simulated elements. Excluding Ω, a remarkable orbital element estimation can be seen after two revolutions. The estimation of Ω is difficult. Due to the relatively low inclination of GRO orbit, the satellite stays in a region where a large change in Ω has little effect on the measured magnetic field magnitude. This stems from the near dipole characteristics of the magnetic field. Due to the circularity of the GRO orbit, ω and θ are not observable separately; only their

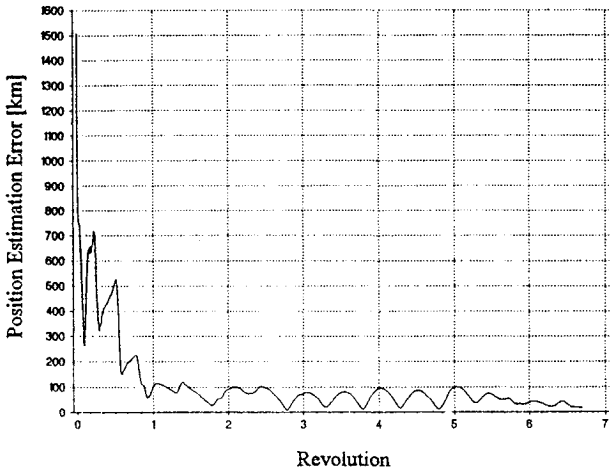

Fig. 9 Position estimation error (augmented basic algorithm operating on GRO data).

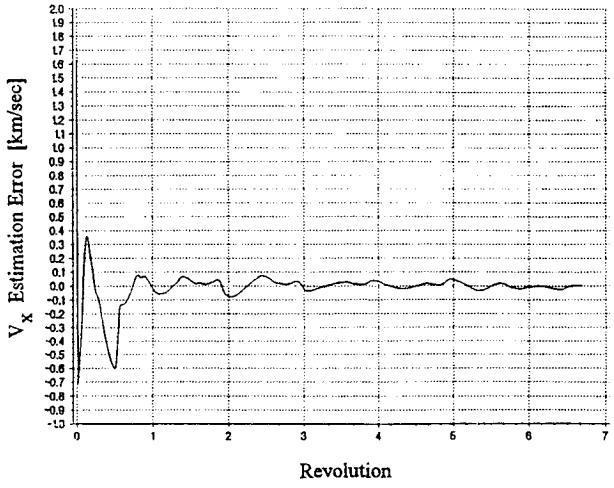

Fig. 10 Estimation error of V_x (augmented basic algorithm operating on GRO data).

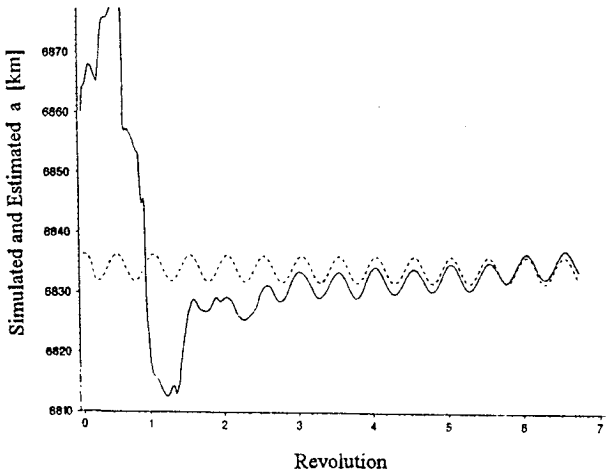

Fig. 11a Simulation and estimation of a (augmented basic algorithm operating on GRO data).

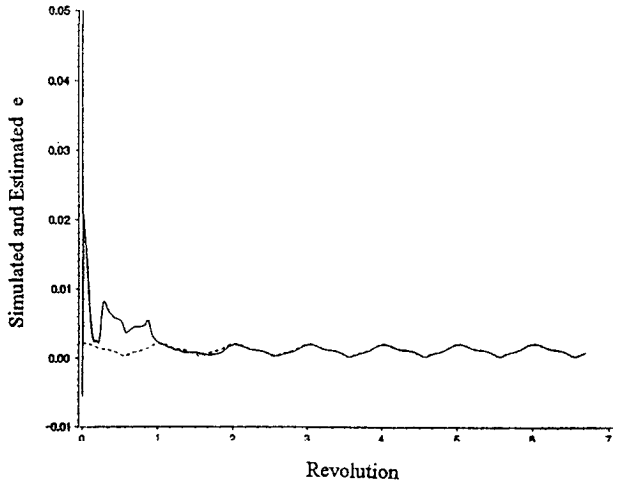

Fig. 11b Simulation and estimation of e (augmented basic algorithm operating as GRO data).

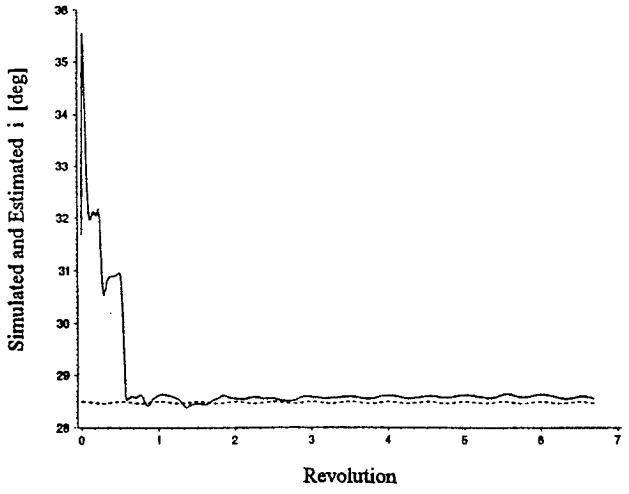

Fig. 11c Simulation and estimation of i (augmented basic algorithm operating on GRO data).

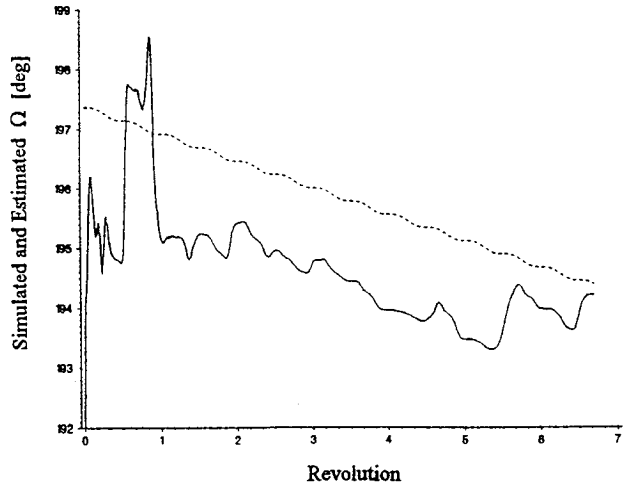

Fig. 11d Simulation and estimation of Ω (augmented basic algorithm operating on GRO data).

sum is. Therefore only the sum of ω and θ (known as the argument of latitude) is presented in Fig. 11e.

2. *Results of Augmented Algorithm with Attitude Information*

Application of the augmented algorithm using attitude information resulted in an identification of the disturbance in the magnetic field component measurement. Consequently, the impressive position estimation error presented in Fig. 12 was obtained. In comparison with the results of the augmented basic algorithm, a considerable improvement can be seen in the transient phase. After the third revolution the error stayed within 10–35 km. It seems to be near the steady-state level of the position error. The main contribution to the improvement in the position estimation was the better estimation of

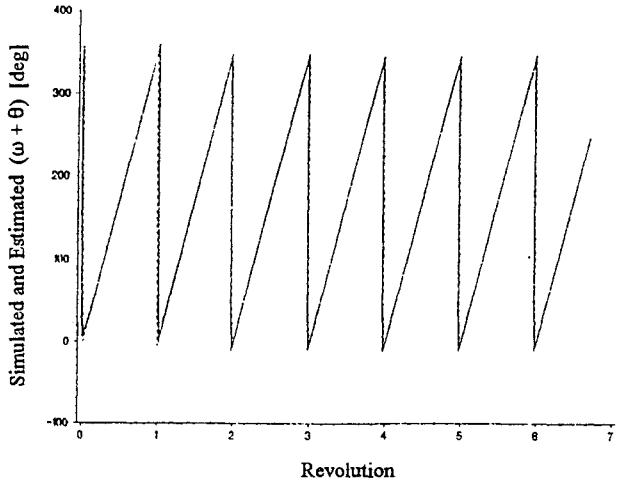

Fig. 11e Simulation and estimation of $\omega + \theta$ (augmented basic algorithm operating on GRO data).

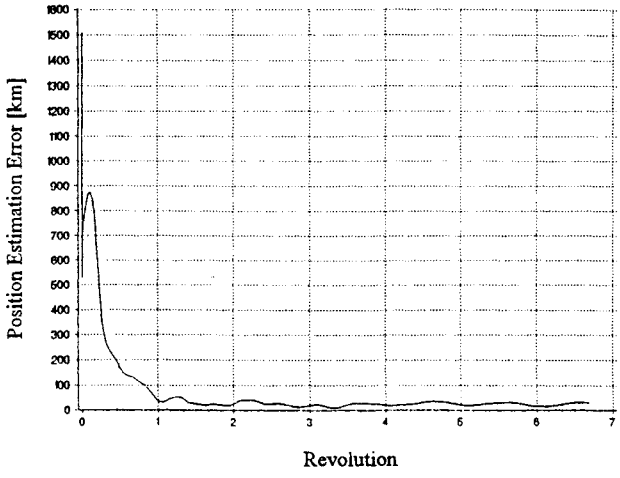

Fig. 12 Position estimation error (augmented algorithm with attitude information operating on GRO data).

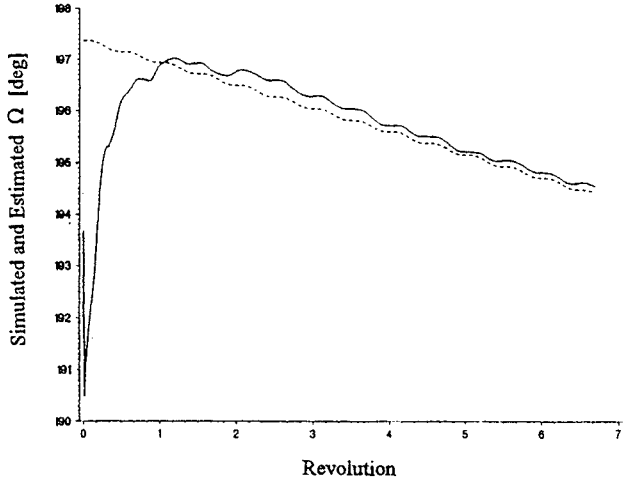

Fig. 13 Simulation and estimation of Ω (augmented algorithm with attitude information operating on GRO data).

Ω obtained with the use of attitude information. This can be seen from a comparison of Fig. 13 with Fig. 11d. (The rest of the orbital elements were estimated quite early in time.)

VI. Conclusions

Near-Earth orbit determination and satellite navigation can be performed using measurements of Earth's magnetic field alone. The method presented in this work has the following advantages: It utilizes magnetometers, which are usually installed on board satellites today anyway for attitude determination, and it is autonomous, independent of ground support or communication with other satellites.

The method is based on instantaneous Keplerian orbital element estimation via the EKF algorithm. Choosing these elements as state variables simplifies the filter implementation.

The navigation algorithms were tested with simulated and real data. Tests with real data are equivalent to on-line true flight tests. The basic navigation algorithm uses a "measurement" of the magnetic field magnitude, which is independent of attitude information. The filter divergence typical of orbit determination problems was eliminated by imposing a lower bound on some of the diagonal elements of the filter covariance matrix. Tests with simulated data resulted in accurate orbital element estimation, yielding around 5 km average position estimation error. Attitude information enabled filter updates using measurements of the magnetic field vector components; in this way three measurements rather than one were used at the update stage of the filter, reducing the average navigation error to a level of 1.8 km and shortening the convergence time considerably. Estimation of the satellite drag coefficient is possible, but the performance improvement is minor in comparison with the increased algorithm complexity. Application of the basic algorithms to two revolutions of measured ERBS data resulted in 30–40 km position error level. When applied to measured GRO data, the basic algorithm was modified in order to handle, recursively, significant biases and low-frequency measurement disturbances. State vector augmentation, which was carried out in order to handle these disturbances, enabled the estimation of the disturbances, which were modeled as a biased first-order Markov sequence. This kind of augmentation may be appropriate to overcome also the significant disturbance that typically occurs during strong magnetic storms. Although GRO orbit is near circular and has a relatively low inclination, its orbital elements were well identified. Position estimation errors between 10 and 35 km were obtained after three revolutions when attitude information was used. It seems that with the current accuracy level of Earth's magnetic field model and the use of internal magnetometers, no better than a few tens of kilometers of navigation errors can be achieved. The actual potential of the autonomous navigation method presented in this paper will be determined conclusively only after additional tests will be carried out with data from more satellites and for long time spans.

A combination of the algorithms presented here with an algorithm that performs attitude determination (see, e.g., Ref. 11), using the same magnetic field measurements, will yield a simple and low-cost autonomous navigation, orbit, and attitude determination system for satellites in near-Earth orbits.

Acknowledgments

We thank J. Teles and T. Stengle of the Flight Dynamics Analysis Branch of NASA Goddard Space Flight Center for authorizing the use of ERBS and GRO data and J. Deutschmann, V. Johnson, S. Greatorex, and D. Baker for supplying the data. We also thank F. Landis Markley, the Associate Editor, and the anonymous reviewers for their helpful remarks.

References

[1]Chory, M. A., Hoffman, D. D., and LeMay, J. L., "Satellite Autonomous Navigation: Status and History," *Proceedings of the IEEE Position, Location and Navigation Symposium* (Las Vegas, NV), Inst. of Electrical and Electronics Engineers, 1986, pp. 110–121.

[2]Psiaki, M. L., and Martel, F., "Autonomous Magnetic Navigation for Earth Orbiting Spacecraft," *Proceedings of the Third Annual AIAA/USU Conference on Small Satellites*, Logan, UT, Sept. 1989.

[3]Fox, S. M., Pal, P. K., and Psiaki, M. L., "Magnetometers-Based Autonomous Satellite Navigation (MAGNAV)," American Astronautical Society, AAS Paper 90-051, 1990.

[4]Psiaki, M. L., Huang, L., and Fox, S. M.,"Ground Tests of Magnetometer Based Autonomous Navigation (MAGNAV) for Low-Earth-Orbiting Spacecraft," *Journal of Guidance, Control, and Dynamics*, Vol. 16, No. 1, 1993, pp. 206–214.

[5]Kaplan, M. H., *Modern Spacecraft Dynamics and Control*, Wiley, New York, 1976.

[6]Jacobs, J. A. (ed.), *Geomagnetism*, Academic, New York, 1987.

[7]Gelb, A. (ed.), *Applied Optimal Estimation*, MIT Press, Cambridge, MA, 1982.

[8]Shorshi, G., and Bar-Itzhack, I. Y., "Satellite Autonomous Navigation Based on Magnetic Field Measurements," Faculty of Aerospace Engineering, Technical Rept. TAE 714, Technion—Israel Inst. of Technology, Haifa, Israel, April 1994.

[9]Jazwinski, A. H., *Stochastic Processes and Filtering Theory*, Academic, New York, 1970.

[10]Bar-Itzhack, I. Y., and Shorshi, G., "Near Earth Orbit Determination Using Magnetometers," *First ESA International Conference on Spacecraft Guidance, Navigation and Control Systems*, Noordwijk, The Netherlands, 1991, pp. 345–350.

[11]Psiaki, M. L., Martel, F., and Pal, P. K., "Three-Axis Attitude Determination via Kalman Filtering of Magnetometer Data," *Journal of Guidance, Control, and Dynamics*, Vol. 13, No. 3, 1990, pp. 506–514.